Title

Identification of differentially expressed proteins involved in fetal scarless wound healing using a rat model of cleft lip

Journal

Molecular Medicine Reports, 24(2)

ISSN

1791-2997

Authors

Yan, Yu
Liu, Hong
Yi, Jiarong
et al.

Publication Date

2021-08-01

DOI

10.3892/mmr.2021.12235

Peer reviewed

Identification of differentially expressed proteins involved in fetal scarless wound healing using a rat model of cleft lip

YU YAN[1-3], HONG LIU[2], JIARONG YI[3], ZIZI CHEN[3], JIA CHEN[3], JIANFEI ZHANG[4], KEWA GAO[3,5], SIQI HE[3,5], AIJUN WANG[5], PING JIN[1], FENG HU[6] and JIANDA ZHOU[3]

[1]Department of Endocrinology, The Third Xiangya Hospital, Central South University, Changsha, Hunan 410013; [2]Department of Nephrology, The Second Xiangya Hospital, Central South University, Changsha, Hunan 410011; [3]Department of Plastic and Reconstructive Surgery, The Third Xiangya Hospital, Central South University, Changsha, Hunan 410013; [4]Department of Burns and Plastic Surgery, The Second Hospital of South China University, Hengyang, Hunan 421000, P.R. China; [5]Department of Surgery, Surgical Bioengineering Laboratory, University of California Davis, Sacramento, CA 95817, USA; [6]Department of Dermatology, Hunan People's Hospital, The First Affiliated Hospital of Hunan Normal University, Changsha, Hunan 410000, P.R. China

Received May 6, 2020; Accepted December 7, 2020

DOI: 10.3892/mmr.2021.12235

Abstract. In early pregnancy, fetal skin wounds can heal quickly and undergo a transition period from scarless healing to scar formation. The aim of the present study was to identify potential biomarkers associated with scarless repair of cleft lips, in order to determine the intrinsic factors leading to scar formation in embryonic tissue. A stable model of cleft lip was established using microsurgery by constructing a wedge-shaped cleft lip-like defect in fetal rats at gestational age (GA) 16.5 and GA18.5. The GA16.5 and GA18.5 groups were used to model scarless healing and scar formation, respectively. The fetuses were returned to the uterus following surgery, then removed 72 h after the procedure. Macroscopic observation of the cleft defect and histological examination were carried out. Reverse transcription-quantitative (RT-q) PCR and parallel reaction monitoring (PRM) were used to detect mRNA and protein expression levels, respectively. The upper-left lip completely healed 72 h after surgery in the GA16.5 group of fetal rats. However, this was not the case in the GA18.5 group. Histological examination indicated new follicles visible under the epidermis of the scarless group (GA16.5). Scarring was visible on the upper-left cleft lip wound of the fetal rats in the GA18.5 group. The expression of some growth and pro-inflammatory factors, including TNF-α, were also different between two groups. Label-free quantification was used to identified differentially expressed proteins and five differentially expressed proteins (Smad4, Fabp5, S100a4, S100a8 and S100a9) were identified. The relative expression of these molecules at the mRNA and protein levels were measured using RT-qPCR and PRM. These molecules may represent potential biomarkers for the scarless repair of fetal rat cleft lip wounds.

Correspondence to: Dr Jianda Zhou, Department of Plastic and Reconstructive Surgery, The Third Xiangya Hospital, Central South University, 138 Tongzipo Road, Changsha, Hunan 410013, P.R. China
E-mail: zhoujianda@csu.edu.cn

Dr Feng Hu, Department of Dermatology, Hunan People's Hospital, The First Affiliated Hospital of Hunan Normal University, 61 Western Jiefang Road, Changsha, Hunan 410000, P.R. China
E-mail: doctorzhoujianda@163.com

Key words: cleft lip, scarless healing, label-free quantification, proteomics, parallel reaction monitoring

Introduction

The cleft lip is a very common congenital oral and maxillofacial malformation, often accompanied by cleft palate and alveolar cleft. Although surgical repair techniques are continuously being improved, numerous patients still experience inevitable secondary scar formation after surgery. In recent years, with the development of prenatal diagnosis and treatment technology (1), intrauterine surgery has made it possible to correct developmental deformities, such as a cleft lip.

The concept of scarless healing was first proposed by Burrington (2) in 1971. It was later observed that fetal skin wounds that occur during early pregnancy can heal quickly and restore intact skin barrier functions. In contrast, fetal skin damage that occurs in the third trimester of pregnancy can result in the formation of scar tissue similar to that of an adult (3). Therefore, the different manifestations of scarless healing of mammalian fetal wounds are related to the gestational age of the fetus (4). Dang *et al* (5) and Longaker *et al* (6) demonstrated that this transition period from scarless healing to scar formation occurred between day 16.5 of gestational age (GA) and GA18.5 in rats and mice, which have a gestation period of ~21.5 days. Lorenz *et al* (7) and Cass *et al* (8) suggested that when 1-2 mm incisions are inflicted on fetal rats, the transition

period of scarless healing to healing with scar formation was still between 16.5 (GA16.5) and 18.5 days (GA18.5).

This phenotypic difference in fetal wounds has inspired further examination of the specific underlying mechanisms. Initially, it was hypothesized that the reason for early scar repair was that the fetus developed in amniotic fluid, which is rich in growth factors and extracellular matrix (ECM) components (9,10). Previous studies typically utilized large animal models to study the presence of scars following repair (11,12). However, only a few studies have reported the use of a fetal rat cleft lip wound model to establish the effectiveness of surgical repair at different gestational ages. Moreover, due to the short gestation period of rats, the experimental cycle can be shortened, and the experiment can therefore be repeated.

Given the importance of this process, the present study, screened out several specific markers of early fetal scarless repair. The present study aimed to gain insight into the occurrence and mechanisms of scarless repair, and to identify new clinical targets for the prevention and treatment of scars.

Materials and methods

Animals. A total of 36 SPF-grade adult Sprague-Dawley (SD) rats (female; mean weight, 250 g; age, 12 weeks) were obtained from the Third Xiangya Hospital of Central South University Animal Experiment Center (Hunan, China) and divided into two groups that received surgery once their fetuses reached GA16.5 or GA18.5, respectively (n=18 each). The following housing conditions were implemented: A temperature between 25±2˚C, relative humidity of 55±15%, ventilation rate of 10-20 times per hour, time-controlled artificial lighting (12-h day-night cycle) and *ad libitum* access to food and water. The experiments were supervised throughout and were performed in accordance with animal experimentation ethics.

Preliminary study on different repair modes applicable to fetal rats with artificial cleft lip wounds. Fetal rats located away from the uterine horn were selected to prevent subsequent abortion, as described previously (13). In the current study, rats were anesthetized with 30 mg/kg pentobarbital sodium intraperitoneally before surgery. A wedge-shaped cleft-like defect was created on the upper-left lip of the fetal rats. The upper-right lip did not receive any treatment and was used as a control condition. The fetal rats were then returned to the uterus. Fetal rats from the GA16.5 and GA18.5 groups were then removed three days post-surgery as previously described (4) (i.e., at GA19.5 or GA21.5, respectively). All fetuses and rats were euthanized using carbon dioxide (30% volume displaced/min). Death was confirmed using cervical dislocation. A total of three fetal rats were obtained from each pregnant rat, for a total of 54 fetal rats from both GA16.5 and GA18.5 groups, and the survival rate was calculated. Tissue samples from the surgical site on the upper-left lip and asymmetrical sections from the upper-right lip were collected from the fetal rats for histological examination, including hematoxylin and eosin (H&E) staining, Masson's Trichrome staining and type-I collagen immunohistochemical staining as previously described (14-16).

The upper-left lip tissue samples from the GA16.5 group were defined as group 1, whereas the upper-right lip tissue samples from the GA16.5 group were defined as group 2. In addition, the upper-left lip tissue samples from the GA18.5 group were defined as group 3, whereas the upper-right lip tissue samples from the GA18.5 group were defined as group 4. Each subgroup included 27 samples. Protein expression was compared between group 1 and 2, group 3 and 4, as well as group 3 and 1. Label-free quantification PRM was performed as previously described (17) and was used to detect the differentially expressed proteins among the different groups. MaxQuant 1.5.6 (https://www.maxquant.org) and Perseus 1.4 (https://www.maxquant.org/perseus/) were used to analyze the results of label-free quantification PRM: Volcano plots were generated for differentially expressed proteins: Y-axis, -log10(P-value); x-axis: log2(ratio). The points distributed outside the two vertical borders and above the horizontal border represented the proteins with significant differences; proteins with at least a 1.5-fold change in expression and $P<0.05$ were considered significant. Subsequently, bioinformatics analysis, including GO and KEGG pathway analysis, was performed to identify differentially expressed proteins (18).

Experimental verification of tissue repair proteins in fetal rats with artificial cleft lip wounds. The mRNA levels of the differentially expressed molecules were assessed using reverse transcription-quantitative (RT-q) PCR, as previously described (19). Differentially expressed levels of proteins were detected by label-free quantification PRM as previously described (17).

Statistical analysis. GraphPad Prism 8.0 (GraphPad Software, Inc.) and SPSS 22.0 (IBM Corp.) were used to perform calculations and carry out statistical analysis. Student's t-test was used to compare differences between two groups. The experimental data from each group were analyzed for congruence of variance before the t-test were applied. The FDR values were within 0.01 in the comparisons. Mixed ANOVA followed by Sidak's post hoc test was used to analyze the differences between multiple groups. $P<0.05$ was considered to indicate a statistically significant difference.

Results

Gross observation. All fetal rats were observed before delivery. The nasolabial cleft was first observed before surgery and images were captured to facilitate the observation of changes in the fetal rats from the GA16.5 and GA18.5 groups. We observed the same area again 72 h post-surgery to identify differences. The cuneiform tissue of the upper-left lip was removed by microsurgery to create a cleft lip wound. The changes in the fetal rats were observed macroscopically. In the GA16.5 group, the upper-left cleft lip wound completely healed 72 h after surgery (i.e., GA19.5) and the continuity of the upper lip tissue was restored. Only a slight depression was observed in the surgical area. The upper-left lip tissue was nearly symmetrical with that of the right side. However, in the GA18.5 group, the cleft lip wound was not completely healed 72 h after surgery (i.e., GA21.5); a clear scar was observed in the surgical area, and the upper lip was asymmetrical on both sides due to wound contracture (Fig. 1).

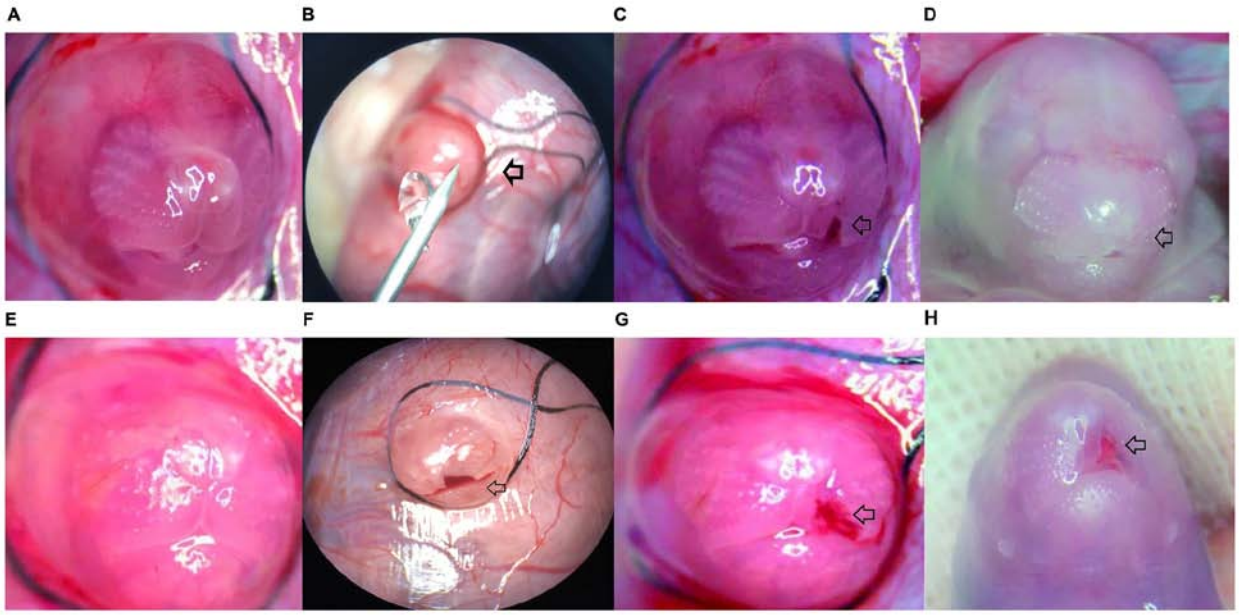

Figure 1. Macroscopic appearance of the cleft lip in the GA16.5 and GA18.5 groups. Arrows indicate the surgical site on the upper-left cleft lip of the fetus. (A-D) Macroscopic appearance of the upper-left lip of a fetus from the GA16.5 group (A) prior to surgery, (B) during surgery, (C) immediately after surgery and (D) 72 h after surgery. (E-H) Macroscopic appearance of the upper-left lip of a fetus from the GA18.5 group (E) prior to surgery, (F) during surgery, (G) immediately after surgery and (H) 72 h after surgery. GA, gestational age.

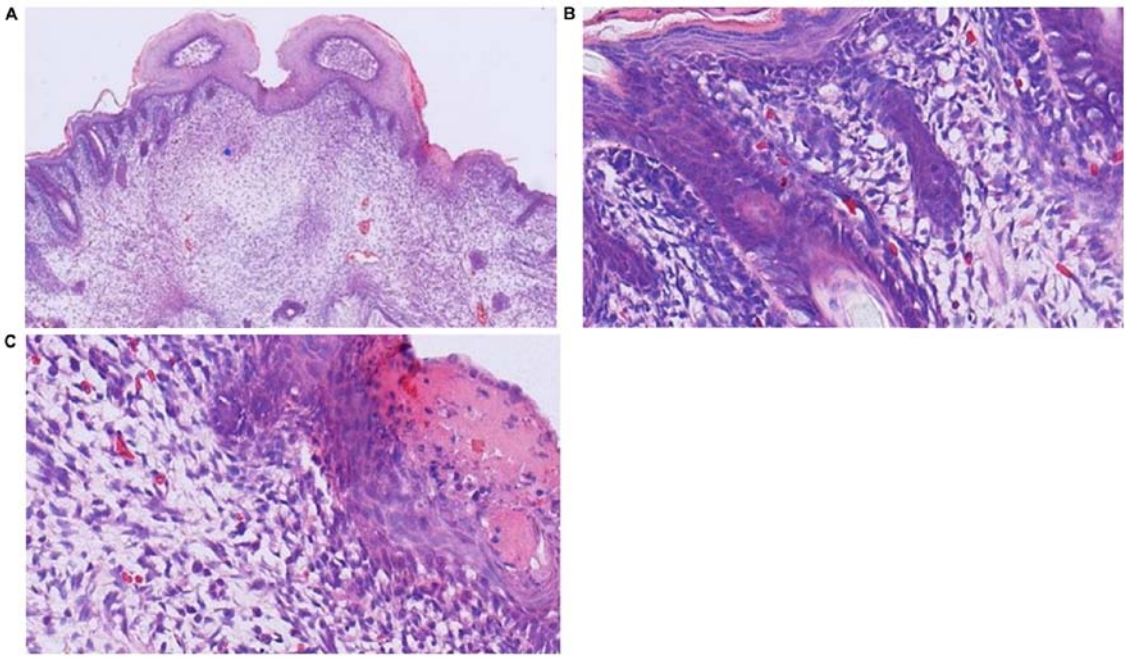

Figure 2. H&E staining of upper lip tissue 72 h following model establishment in the GA16.5 group. (A) H&E staining of the upper lip tissue. The slight depression in the upper-left lip identifies the location where the cleft lip-like defect was created. The site of the defect is completely epithelialized. Magnification, x40. (B) Normal subepidermal structure of the upper-right lip. Magnification, x400. (C) New follicular structures can be observed under the epidermis of the upper-left lip. Magnification, x400. GA, gestational age; H&E, hematoxylin and eosin.

Histological analysis. In the GA16.5 group 72 h after surgery, the tissue of the upper-left lip wound demonstrated complete regeneration when observed under the microscope (Figs. 2-4). The results of H&E staining demonstrated complete epithelialization of the upper-left lip, and the structure of new follicles was detected under the epidermis. Compared with the normal skin of the upper-right lip, a slight depression in the cleft part of the upper-left lip and thickening of the skin was noted, whereas inflammatory cell infiltration and neovascularization were not apparent (Fig. 2). Masson's Trichrome staining revealed collagen fibers under the epidermis, demonstrating a fine reticular and emerging follicular structure (Fig. 3). Immunohistochemical analysis indicated no obvious difference in the amount of type-I collagen in the upper-left cleft lip area and the rest of the upper lip (Fig. 4).

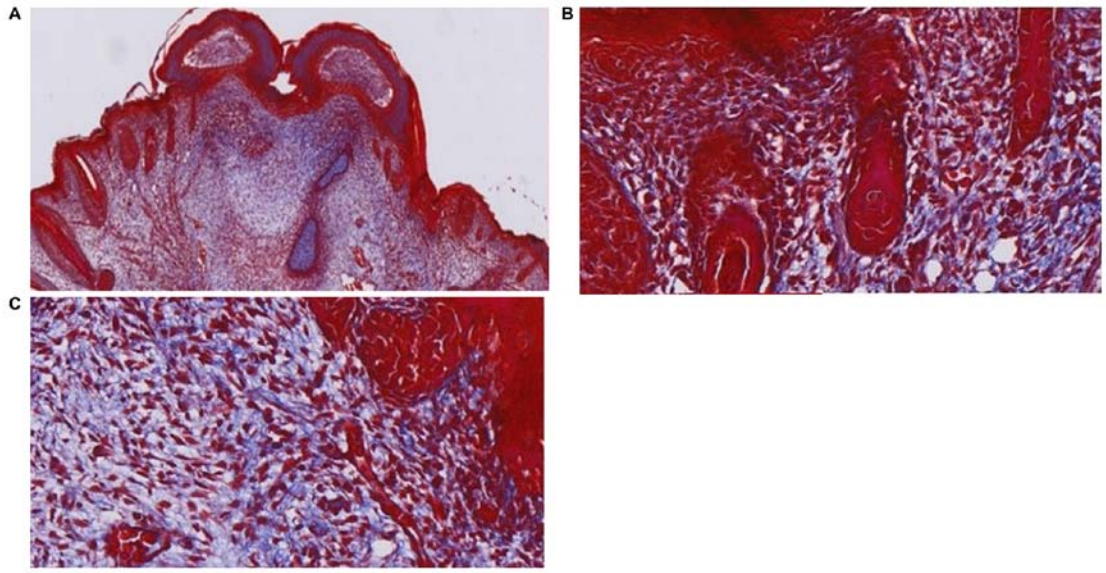

Figure 3. Masson's Trichrome staining 72 h following model establishment in the GA16.5 group. (A) Masson's Trichrome staining of the upper lip tissue. The slight depression in the upper-left lip identifies the location where the cleft lip-like defect was created. Magnification, x40. (B) Normal subepidermal structure of the upper-right lip. Magnification, x400. (C) The fine network of collagen fibers (stained blue) and new hair follicle structures are visible under the epidermis of the upper-left lip. Magnification, x400. GA, gestational age.

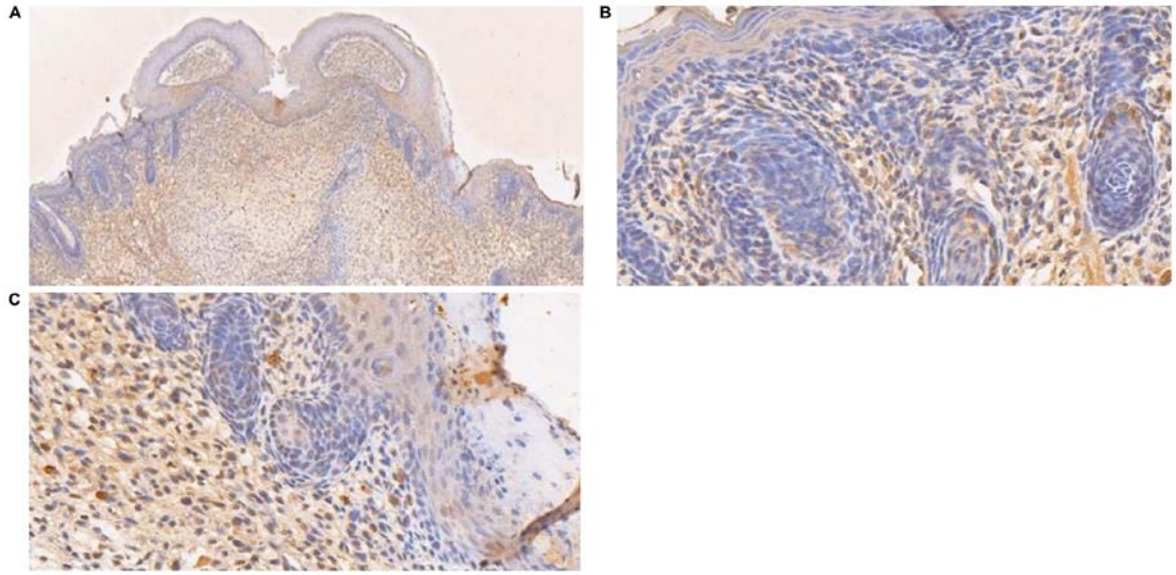

Figure 4. IHC staining 72 h following model establishment in the GA16.5 group. (A) IHC staining of the upper lip tissue. The slight depression in the upper-left lip identifies the location where the cleft lip-like defect was created. Magnification, x40. (B) Normal subepidermal structure of the upper-right lip. Magnification, x400. (C) The expression of type-I collagen in the upper-left lip is almost indistinguishable from the upper-right lip. Magnification, x400. GA, gestational age; IHC, immunohistochemistry.

In the GA18.5 group, the position of the wound was easily identified by a distinct scar on the upper-left lip. H&E staining demonstrated that partial epithelialization occurred in the upper-left cleft lip area. Compared with the normal skin of the upper-right lip, the upper-left lip displayed a clear scar, new capillary formation around the wound and increased fibroblast proliferation and ECM volume, whereas structural components of hair follicles were not observed under the epidermis (Fig. 5). Masson's Trichrome staining demonstrated the absence of new follicular structure and the presence of dense collagen fibers under the epidermis (Fig. 6). Immunohistochemical analysis in the upper-left cleft lip wound demonstrated an increase in type-I collagen expression and fiber density, as well as a more compact structure and absence of adnexal skin (Fig. 7), compared with normal upper lip tissue.

Immunohistochemical analysis of cell proliferation markers was also carried out. Compared with GA16.5 fetal rats, the expression of Ki67 and CD31 slightly increased in the GA18.5 group following surgery. By contrast, the expression of CK10 decreased in the GA18.5 group, compared with the GA16.5 group (Fig. 8).

RT-qPCR analysis of inflammatory factors. The relative mRNA expression levels of the pro-inflammatory factors

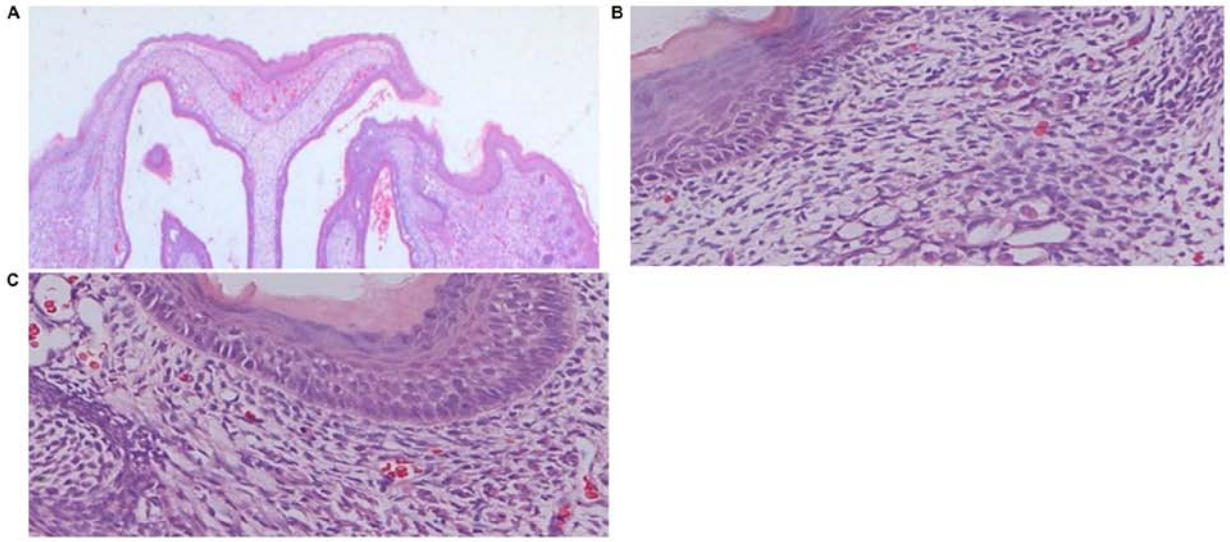

Figure 5. H&E staining of upper lip tissue 72 h following model establishment in the GA18.5 group. (A) H&E staining of the upper lip tissue. A clear depression in the upper-left lip identifies the location where the cleft lip-like defect was created. The site of the defect is not completely healed. Magnification, x40. (B) Normal subepidermal structure of the upper-right lip. Magnification, x400. (C) No new hair follicle structures were observed under the epidermis. New capillaries, an increased number of fibroblasts and an increased volume of extracellular matrix can be observed around the wound. Magnification, x400. GA, gestational age.

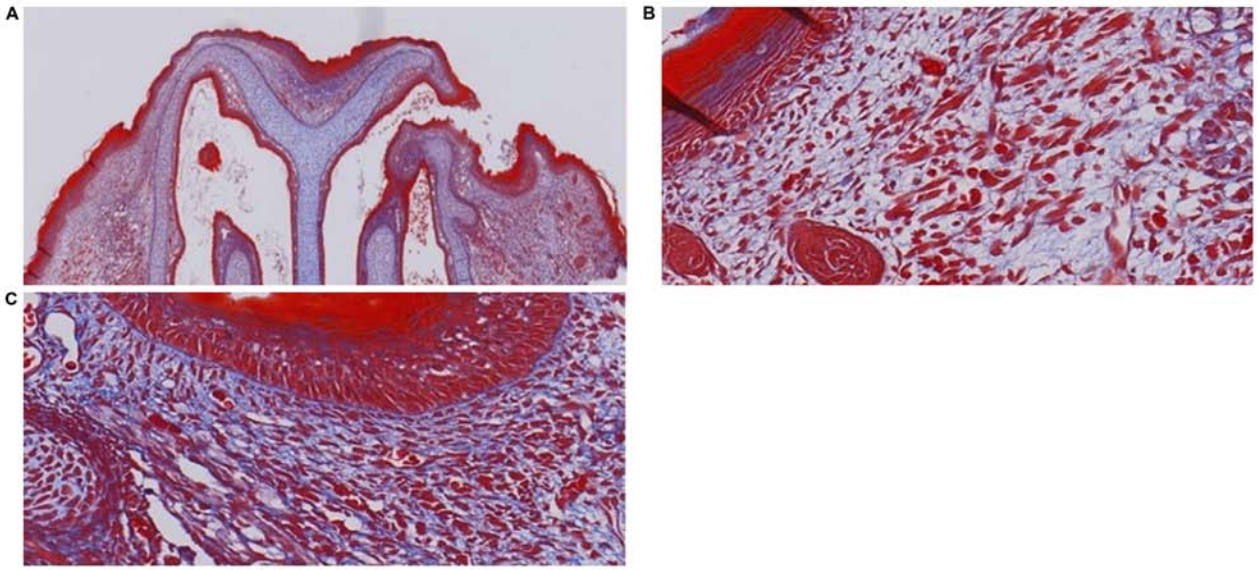

Figure 6. Masson's Trichrome staining 72 h after model establishment in the GA18.5 group. (A) Masson's Trichrome staining of the upper lip tissue. A clear depression in the upper-left lip identifies the location where the cleft lip-like defect was created Magnification, x40. (B) Normal subepidermal structure of the upper-right lip. Magnification, x400. (C) The collagen fibers (stained blue) are visible and no new hair follicle structures are observed under the epidermis of the upper-left lip. Magnification, x400. GA, gestational age.

TNF-α, IL-10 and TGF-β were evaluated in the two groups of fetal rats. The mRNA levels of TNF-α and IL-10 were significantly higher in GA18.5 rats, compared with GA16.5 rats. Furthermore, the mRNA expression levels of TGF-β were significantly reduced in the GA18.5 group (Fig. 9).

Protein identification and differential protein screening. Compared with group 1, 57 differentially expressed proteins were identified in group 2, of which 37 were upregulated and 20 were downregulated. A comparison of groups 3 and 4 revealed 312 differentially expressed proteins, of which 171 were upregulated and 141 were downregulated. Lastly, compared with group 1,289 differentially expressed proteins were identified in group 3, of which 151 were upregulated and 138 were downregulated. Only 50 differentially expressed proteins and their multiple variations were upregulated or downregulated between all groups (Tables I-IV). The distribution of the differentially expressed proteins among the selected samples is presented as volcano plots (Figs. 10-12).

Bioinformatics analysis. Gene ontology (GO) enrichment analysis was performed on the differentially expressed proteins, and their properties were generally described as

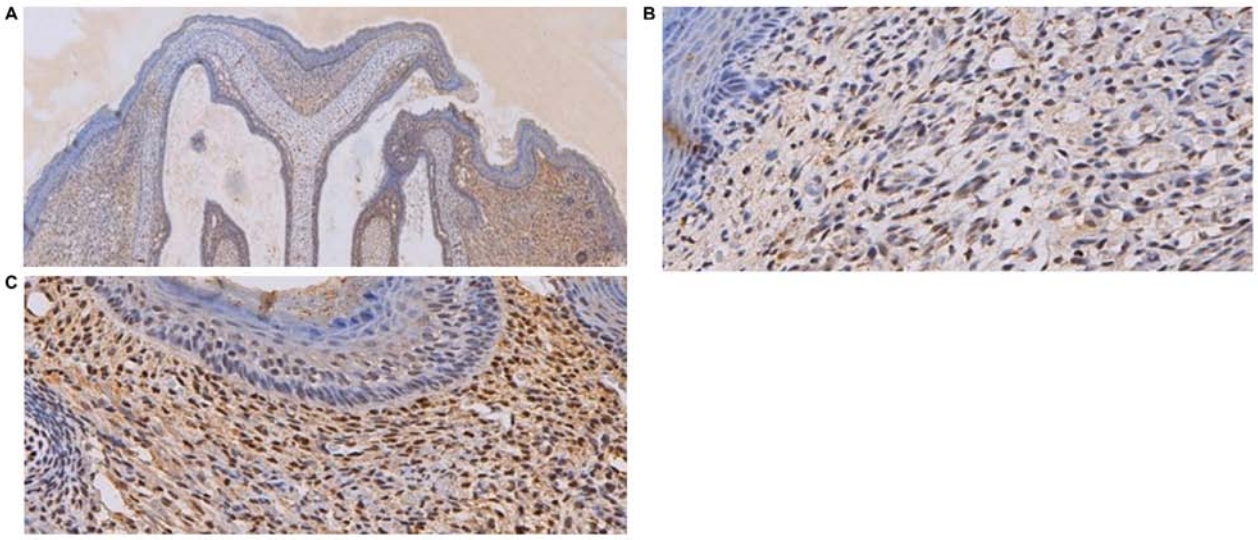

Figure 7. IHC staining 72 h after model establishment in the GA18.5 group. (A) IHC staining of the upper lip tissue. A clear depression in the upper-left lip identifies the location where the cleft lip-like defect was created Magnification, x40. (B) Normal subepidermal structure of the upper-right lip. Magnification, x400. (C) The expression of type-I collagen in the upper-left lip is higher compared with the upper-right lip. Magnification, x400. GA, gestational age; IHC, immunohistochemistry.

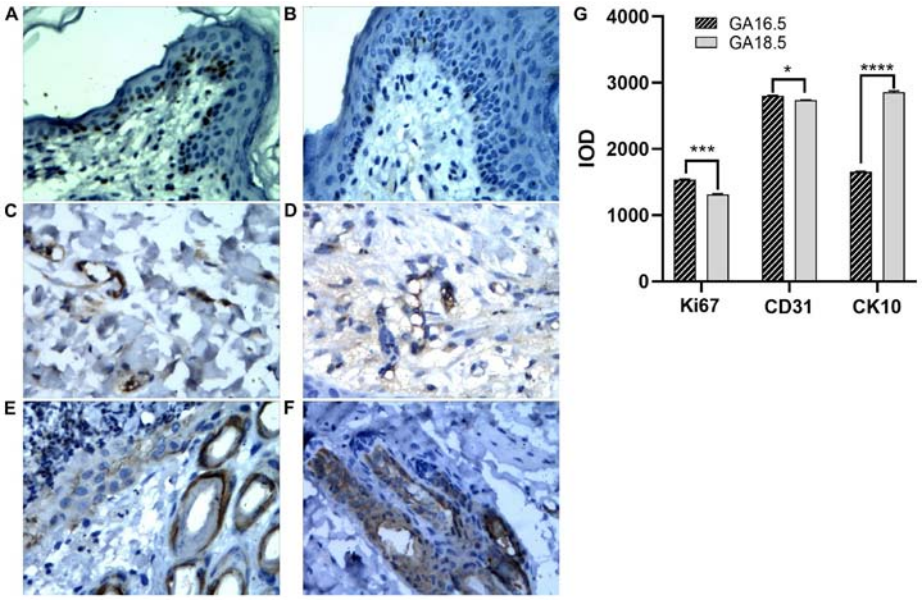

Figure 8. Immunohistochemical analysis 72 h after model establishment in the GA16.5 and GA18.5 groups. (A and B) Ki67 staining of upper lip tissue from (A) the GA16.5 group and (B) the GA18.5 group. (C and D) CD31staining of upper lip tissue from (C) the GA16.5 group and (D) the GA18.5 group. (E and F) CK10 staining of upper lip tissue from (E) the GA16.5 group and (F) the GA18.5 group. (G) IOD values for Ki67, CD31 and CK10 staining in both groups. *P<0.05; ***P<0.001; ****P<0.0001. GA, gestational age; IOD, integral optical density.

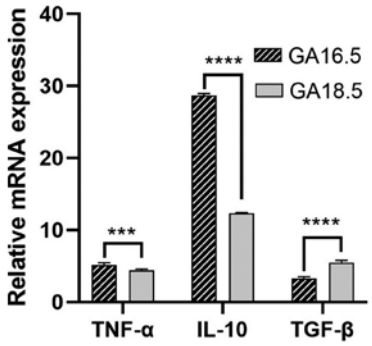

Figure 9. Relative mRNA expression levels of TNF-α, IL-10 and TGF-β. ***P<0.001; ****P<0.0001. GA, gestational age.

biological process (BP), molecular function (MF) or cellular component (CC). The first 10 GO enrichment results from each group are displayed in Fig. 13. The results demonstrated that 73, 542 and 376 differentially expressed proteins were significantly enriched between groups 1 and 2, 3 and 4 and 3 and 1, respectively. The results of the Kyoto Encyclopedia of Genes and Genomes (KEGG) pathway enrichment analysis identified the possible pathway related to the differentially expressed proteins between groups (Fig. 14).

In addition, the interaction network of the differentially expressed proteins that regulate wound repair were analyzed. Examples of the interaction networks of the differentially expressed proteins involved in wound repair are as follows:

Table I. Comparison of differentially expressed protein numbers between samples.

Sample	Differentially expressed proteins, n	Upregulated proteins, n	Downregulated protein, n
Group 1 vs. Group 2	57	37	20
Group 3 vs. Group 4	312	171	141
Group 3 vs. Group 1	312	151	138

Group 1, upper-left lip without scar repair group at 72 h after modeling in GA16.5 rats; Group 2, upper-right lip normal group at 72 h after modeling in GA16.5 rats; Group 3, upper-left lip scar repair group at 72 h after modeling in GA18.5 rats; Group 4, upper-right lip normal group at 72 h after modeling in GA18.5 rats.

Table II. Differential protein expression in group 1 and group 2.

Protein ID	Gene name	Protein name	P-value	Fold-change
G3V8R3	Hbz	Hemoglobin, zeta	0.004	7.788
B2RYS8	Ndufb8	NADH dehydrogenase	0.000	5.024
Q920P6	Ada	Adenosine deaminase	0.038	4.831
O88752	Hbe1	Hemoglobin, epsilon 1	0.003	4.801
Q499N7	Ptpn6	Tyrosine-protein phosphatase non-receptor type 6	0.003	4.700
Q4FZU2	Krt6a	Keratin 6A	0.001	4.044
P06762	Hmox1	Heme oxygenase 1	0.011	3.902
Q6IFU9	Krt16	Keratin, type I cytoskeletal 16	0.006	3.613
Q99PD6	Tgfb1i1	Transforming growth factor beta-1-induced transcript 1 protein	0.004	3.590
Q6P7S1	Asah1	Acid ceramidase	0.029	3.167
Q63066	Hbg1	Hemoglobin, gamma A	0.002	3.082
Q10758	Krt8	Keratin, type II cytoskeletal 8	0.004	2.901
Q6AYQ4	Tmem109	Transmembrane protein 109	0.048	2.710
Q9Z2Q7	Stx8	Syntaxin-8	0.035	2.660
G3V9M8	Fam50a	Protein fam50a	0.034	2.515
M0R9Y3	Nup43	Nucleoporin 43	0.005	2.461
B2GVB9	Fermt3	Fermitin family homolog 3	0.018	2.425
G3V8H	Olfml3	Olfactomedin-like protein 3 precursor	0.045	2.383
D4A531	Polr2i	Rna polymerase ii subunit i	0.049	2.290
Q68FS1	Nubp2	Cytosolic Fe-S cluster assembly factor	0.028	2.221
D3ZLS5	Hectd1	Hect domain e3 ubiquitin protein ligase 1	0.033	2.112
D4A0M2	Nxn	Nucleoredoxin	0.033	2.056
Q6IE17	Stfa2l2	Stefin-3	0.007	1.969
P27139	Ca2	Carbonic anhydrase 2	0.032	1.957
D3ZF44	LOC684499	Protein LOC684499	0.015	1.940
Q6LDZ3	Ptprc	Receptor-type tyrosine-protein phosphatase C	0.007	1.878
Q5XI38	Lcp1	Plastin-2	0.018	1.843
Q5PPG2	Lgmn	Legumain precursor	0.015	1.820
P06765	Pf4	Platelet factor 4	0.050	1.708
Q9R1T3	Ctsz	Cathepsin Z	0.011	1.707
Q5U1Y2	Rac2	Ras-related C3 botulinum toxin substrate 2	0.021	1.669
Q5U2V4	Plbd1	Phospholipase B-like 1	0.028	1.630
Q9EPX0	Hspb8	Heat shock protein beta-8	0.005	1.603
O35532	Msmo1	Methylsterol monooxygenase 1	0.037	1.592
Q91ZN1	Coro1a	Coronin-1A	0.013	1.586
O88201	Clec11a	C-type lectin domain family 11 member A	0.025	1.547
Q5U329	Slc4a1	Band 3 anion transport protein	0.027	1.512
Q496Z5	Prph	Peripherin	0.041	0.626
P19527	Nefl	Neurofilament light polypeptide	0.040	0.608

Table II. Continued.

Protein ID	Gene name	Protein name	P-value	Fold-change
Q9ESI7	Dcx	Neuronal migration protein doublecortin	0.003	0.597
Q6AY98	Ube2e2	Ubiquitin conjugating enzyme e2 e2	0.046	0.577
Q7TSX7	Nr3c1;gr	Glucocorticoid receptor	0.026	0.560
O70437	Smad4	Mothers against decapentaplegic homolog 4	0.043	0.557
F1M754	Map4k4	Mitogen-activated protein kinase kinase kinase kinase 4	0.022	0.526
D4A2Z8	Dhx36	Probable ATP-dependent RNA helicase DHX36	0.009	0.522
P31430	Dpep1	Dipeptidase 1	0.010	0.513
Q6AXY8	Dhrs1	Dehydrogenase/reductase SDR family member 1	0.019	0.495
D4A414	Cox15	COX15 homolog	0.031	0.476
D4ABV5	Calm1	Calmodulin 1	0.012	0.473
D3ZRN3	Actbl2	Beta-actin-like protein 2	0.048	0.413
Q8CGS4	Chmp3	Charged multivesicular body protein 3	0.022	0.410
D3ZHA7	Myl6b	Myosin light chain 6b	0.011	0.390
P70541	Eif2b3	Translation initiation factor eif-2B subunit gamma	0.002	0.324
D3ZX50	Krtap11-1	Uncharacterized protein	0.037	0.287
D3ZD07	Fmo9	Flavin containing monooxygenase 9 pseudogene	0.007	0.277
Q6IFX1	Krt24	Keratin, type I cytoskeletal 24	0.012	0.050
Q6IG02	Krt2	Keratin, type II cytoskeletal 2	0.008	0.021

Group 1: Upper-left lip of fetus at 72 h after modeling in GA16.5 rats; Group 2, upper-right lip of fetus at 72 h after modeling in GA16.5 rats. GA, gestational age.

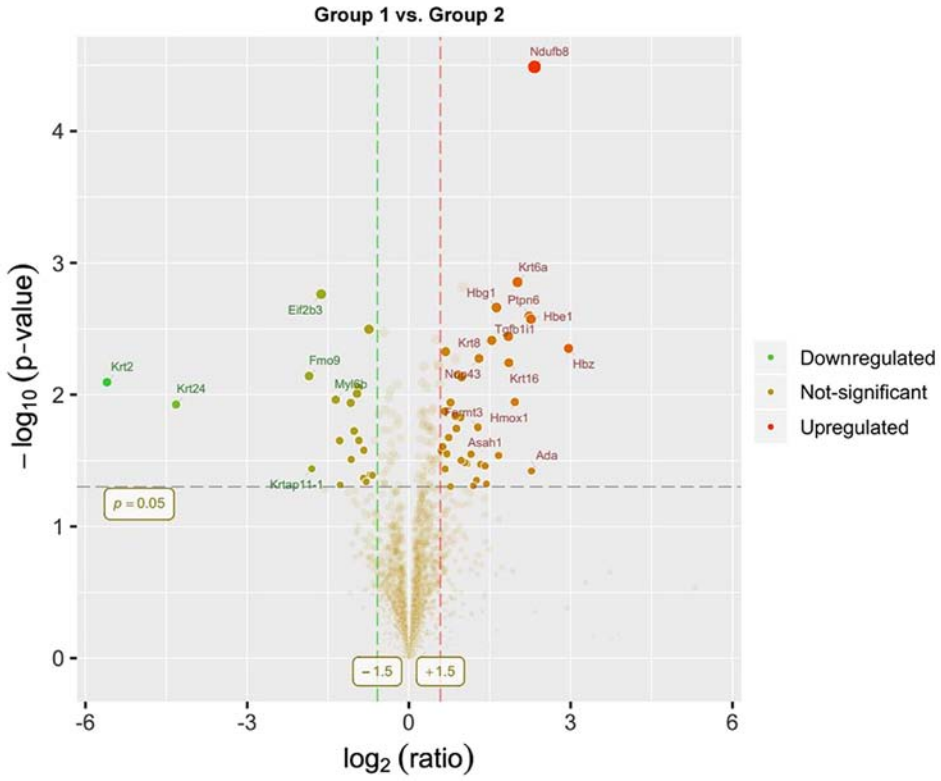

Figure 10. Volcano plot of the differentially expressed proteins in group 1 and group 2. Group 1, upper-left lip of fetus at 72 h after modeling in GA16.5 rats; Group 2, upper-right lip of fetus at 72 h after modeling in GA16.5 rats. GA, gestational age.

i) Smad4, Tgf1i1, Ptpn6 and Hmox1 in group 1 and 2; ii) S100a9, Fgg, Anxa1, Fgb, Plg and S100a8 in group 3 and 4; and iii) CD36, S100a9, S100a8, Cd9Fgg, Anxa1, Fgb, Plg and S100a8 in group 3 and 1 (Fig. 15).

Table III. Differential protein expression in group 3 and group 4.

Protein ID	Gene name	Protein name	P-value	Fold change
D3ZGE2	Mpo	Myeloperoxidase	0.000	377.923
Q62714	Np4	Neutrophil antibiotic peptide NP-4	0.000	231.771
D3ZY96	Ngp	Neutrophilic granule protein precursor	0.010	226.724
P50115	S100a8	S100 Calcium Binding Protein A8	0.001	92.828
Q7TP54	Fam65b	Protein FAM65B	0.000	77.718
D3ZMI6	Olfm4	Olfactomedin-4 precursor	0.001	63.833
D4A081	Setdb1	Histone-lysine N-methyltransferase SETDB1	0.000	47.032
Q9JI30	Itgam	Integrin alpha-M precursor	0.011	39.489
B2RYB8	Itgb2	Integrin beta 2 precursor	0.003	34.443
P50116	S100a9	S100 Calcium Binding Protein A9	0.000	30.191
Q920P6	Ada	Adenosine deaminase	0.028	27.433
Q499N7	Ptpn6	Tyrosine-protein phosphatase non-receptor type 6	0.003	23.157
Q9ERL1	Cybb	Cytochrome b-245, beta polypeptide	0.002	21.484
Q9JKB7	Gda	Guanine deaminase	0.019	20.202
Q5U1Y2	Rac2	Ras-related C3 botulinum toxin substrate 2	0.007	19.291
Q6IFU9	Krt16	Keratin, type I cytoskeletal 16	0.001	13.524
O54854	Klk6	Kallikrein-6 precursor	0.000	11.605
B2GVB9	Fermt3	Fermitin family homolog 3	0.012	11.176
Q5PQW8	Gbp2	Interferon-induced guanylate-binding protein 2	0.019	10.854
Q6LDZ3	Ptprc	Receptor-type tyrosine-protein phosphatase C	0.015	10.626
Q4G075	Serpinb1a	Leukocyte elastase inhibitor A	0.001	9.051
Q6PDV1	Lyz1	Lysozyme C-1 precursor	0.002	9.049
Q6IE17	Stfa2l2	Stefin-3	0.000	8.930
Q5U2V4	Plbd1	Phospholipase B-like 1	0.003	8.669
Q91ZN1	Coro1a	Coronin-1A	0.001	8.199
P14669	Anxa3	Annexin A3	0.008	8.100
Q9R0D6	Tcn2	Transcobalamin-2 precursor	0.014	7.286
Q4QQV6	Lsp1	Lymphocyte specific 1	0.004	6.785
P06768	Rbp2	Retinol-binding protein 2	0.006	6.051
Q5XI38	Lcp1	Plastin-2	0.001	5.841
Q91W30	Akr1b8	Aldo-Keto Reductase Family 1 Member B8	0.001	5.492
Q63015	Csap1	Common salivary protein 1 precursor	0.001	5.454
P31720	C1qa	Complement C1q subcomponent subunit A	0.008	5.339
G3V904	Pld4	Phospholipase D4	0.005	4.857
D4ADD7	Glrx5	Glutaredoxin-related protein 5	0.002	4.782
P22985	Xdh	Xanthine dehydrogenase/oxidase	0.003	4.221
P06866	Hp	Haptoglobin Haptoglobin alpha chain Haptoglobin beta chain	0.002	3.945
B2RYS9	Trmt112	Uncharacterized protein	0.016	3.827
P23640	Rab27a	Ras-related protein Rab-27A	0.017	3.774
P06762	Hmox1	Heme oxygenase 1	0.008	3.769
Q9WUQ4	Slpi	Secretory leukocyte peptidase inhibitor precursor	0.015	3.710
P07150	Anxa1	Annexin A1	0.003	3.449
D3ZX79	Ly6g6c	Lymphocyte antigen 6 complex G6C precursor	0.018	3.236
O88752	Hbe1	Hemoglobin, epsilon 1	0.029	3.211
Q9R1T3	Ctsz	Cathepsin Z	0.002	3.195
D3ZJH9	Me2	NAD-dependent malic enzyme, mitochondrial	0.034	2.926
P05942	S100a4	S100 Calcium Binding Protein A4	0.002	2.897
Q5XJW6	Cfh	Complement factor H precursor	0.008	2.891
O54892	Hk2	Hexokinase-2	0.007	2.876
Q6P7D4	Cyp20a1	Cytochrome P450 20A1	0.013	0.490
D3ZWC6	Sntb1	beta-1-syntrophin	0.025	0.490
Q62997	Gfra1	GDNF family receptor alpha-1	0.043	0.488

Table III. Continued.

Protein ID	Gene name	Protein name	P-value	Fold change
P02600	Myl1	Myosin light chain 1/3	0.011	0.482
O35878	Hspb2	Heat shock protein beta-2	0.005	0.481
P17209	Myl4	Myosin light chain 4	0.004	0.475
D4A8H3	Uba6	Ubiquitin-like modifier-activating enzyme 6	0.031	0.471
A1L1K3	Anapc5	Anaphase-promoting complex subunit 5	0.046	0.470
D3ZTW9	Exog	Nuclease EXOG	0.028	0.467
D4A3D2	Smyd1	SET and MYND domain-containing protein 1	0.004	0.465
P04466	Mylpf	Myosin regulatory light chain 2	0.009	0.464
P12847	Myh3	Myosin-3	0.007	0.461
P13413	Tnni1	Troponin I	0.001	0.460
D4A4Y2	Hsd17b14	17-beta-hydroxysteroid dehydrogenase 14	0.033	0.455
P23928	Cryab	Alpha-crystallin B chain	0.020	0.454
Q7TNB2	Tnnt1	Troponin T	0.002	0.451
D3ZCD7	Tp53rk	TP53-regulating kinase	0.004	0.450
P00564	Ckm	Creatine kinase M-type	0.037	0.450
Q80W59	Hrc	Sarcoplasmic reticulum histidine-rich calcium-binding protein precursor	0.019	0.445
P50463	Csrp3	Cysteine and glycine-rich protein 3	0.013	0.444
Q5XIG1	Ldb3	Ldb3 protein	0.017	0.443
D3ZUB7	Anapc4	Anaphase-promoting complex subunit 4	0.030	0.442
Q64578	Atp2a1	ATPase, Ca++ transporting, cardiac muscle, fast twitch 1	0.032	0.442
Q6P792	Fhl1	Four and a half LIM domains protein 1	0.013	0.431
Q8K4F2	Alox15b	Arachidonate 15-lipoxygenase B	0.025	0.428
M0RBL8	Tceal6	Protein LOC679974	0.003	0.427
P51868	Casq2	Calsequestrin-2 precursor	0.008	0.425
B4F789	Apobec2	Probable C->U-editing enzyme APOBEC-2	0.008	0.421
P16290	Pgam2	Phosphoglycerate mutase 2	0.014	0.418
Q9Z2J4	Nexn	Nexilin	0.002	0.412
Q9QYU4	Crym	Thiomorpholine-carboxylate dehydrogenase	0.017	0.411
D3ZUQ0	Rilpl1	RILP-like protein 1	0.006	0.409
D4A2H6	Rbfox3	Fox-1 homolog C	0.037	0.408
D3ZVM5	Hspa12b	Heat shock 70 kDa protein 12B	0.038	0.406
O54747	Pold1	DNA polymerase delta catalytic subunit	0.001	0.403
P52481	Cap2	Adenylyl cyclase-associated protein 2	0.007	0.396
Q63544	Sncg	Gamma-synuclein	0.004	0.381
Q496Z5	Prph	Peripherin	0.001	0.376
P07483	Fabp3	Fatty acid-binding protein, heart	0.011	0.357
P23565	Ina	Alpha-internexin	0.005	0.332
D4ADS4	Mgst3	Microsomal glutathione S-transferase 3	0.024	0.328
P19527	Nefl	Neurofilament light polypeptide	0.006	0.326
P12839	Nefm	Neurofilament medium polypeptide	0.004	0.326
B2RZ77	Dpt	Dermatopontin precursor	0.024	0.320
Q6AYG3	Prune	Prune homolog	0.017	0.320
G3V7K1	Myom2	Myomesin 2	0.025	0.299
G3V6V5	Atp1b4	Protein ATP1B4	0.005	0.272
Q9Z2Z8	Dhcr7	7-dehydrocholesterol reductase	0.000	0.270
P19633	Casq1	Calsequestrin-1	0.021	0.201
D3ZX18	Myoz2	Myozenin-2	0.001	0.198
Q812D3	Ppil3	Peptidyl-prolyl cis-trans isomerase-like 3	0.000	0.179

Group 3, upper-left lip of fetus at 72 h after modeling in GA18.5 rats; Group 4, upper-right lip of fetus at 72 h after modeling in GA18.5 rats. GA, gestational age.

Table IV. Differential protein expression in group 3 and group 1.

Protein ID	Gene name	Protein name	P-value	Fold change
Q6jhy3	Smgc	Submandibular gland protein c precursor	0.001	753.286
D3zge2	Mpo	Myeloperoxidase precursor	0.000	271.832
Q62714	Np4	Neutrophil antibiotic peptide np-4	0.000	244.647
D3zmi6	Olfm4	Olfactomedin-4 precursor	0.000	189.639
D3zy96	Ngp	Neutrophilic granule protein precursor	0.014	130.459
B2ryb8	Itgb2	Integrin beta 2 precursor	0.002	44.874
G3v8l7	Itgam	Integrin alpha-m precursor	0.012	32.024
Q6ig02	Krt2	Keratin, type ii cytoskeletal 2 epidermal	0.011	26.577
Q63015	Csap1	Common salivary protein 1 precursor	0.003	26.571
P50115	S100a8	S100 calcium binding protein a8	0.002	25.933
P50116	S100a9	S100 calcium binding protein a9	0.001	19.538
Q9jkb7	Gda	Guanine deaminase	0.023	19.076
D3zd07	Fmo9	Flavin containing monooxygenase 9 pseudogene	0.003	17.428
Q5u1y2	Rac2	Ras-related c3 botulinum toxin substrate 2	0.011	12.859
O54854	Klk6	Kallikrein-6 precursor	0.000	10.614
Q5u2v4	Plbd1	Phospholipase b-like 1	0.002	10.508
Q6pdv1	Lyz1	Lysozyme c-1 precursor	0.002	8.631
Q4g075	Serpinb1a	Leukocyte elastase inhibitor a	0.001	8.260
Q6ldz3	Ptprc	Receptor-type tyrosine-protein phosphatase c	0.023	8.077
Q9wuq4	Slpi	Secretory leukocyte peptidase inhibitor precursor	0.007	7.093
Q9erl1	Cybb	Cytochrome b-245, beta polypeptide	0.009	7.056
E0a3n4	Serpina3n	Serine protease inhibitor a3n	0.013	7.049
G3v6k1	Tcn2	Transcobalamin-2 precursor	0.017	6.577
P14669	Anxa3	Annexin a3	0.010	5.005
P22985	Xdh	Xanthine dehydrogenase/oxidase	0.003	4.802
Q91zn1	Coro1a	Coronin-1a	0.001	4.694
P05982	Nqo1	Nad(p)h quinone dehydrogenase 1	0.001	4.334
P23640	Rab27a	Ras-related protein rab-27a	0.019	3.830
Q6ifu9	Krt16	Keratin, type i cytoskeletal 16	0.001	3.797
Q62894	Ecm1	Extracellular matrix protein 1	0.039	3.655
Q5xi38	Lcp1	Plastin-2	0.003	3.469
P07150	Anxa1	Annexin a1	0.003	3.446
Q78zr5	Hopx	Homeodomain-only protein	0.002	3.376
P01015	Agt	Angiotensinogen angiotensin-1 angiotensin-2 angiotensin-3	0.010	3.300
Q6axy8	Dhrs1	Dehydrogenase/reductase sdr family member 1	0.006	3.287
Q91w30	Akr1b8	Aldose reductase-related protein 2	0.007	3.244
P32755	Hpd	4-hydroxyphenylpyruvate dioxygenase	0.024	3.149
Q499n7	Ptpn6	Tyrosine-protein phosphatase non-receptor type 6	0.038	3.025
G3v755	Sprr1a	Cornifin-a	0.002	3.006
Q5xfv4	Fabp4	Fatty acid-binding protein, adipocyte	0.024	2.910
B1wbv8	Pld4	Phospholipase d4	0.011	2.909
D3zpf9	Serpinb12	Serpin b12	0.038	2.880
Q4qqv6	Lsp1	Lymphocyte specific 1	0.001	2.665
P29524	Serpinb2	Plasminogen activator inhibitor 2 type a	0.001	2.653
O55162	Lypd3	Ly6/plaur domain-containing protein 3	0.004	2.551
D4a5u3	Tgm3	Protein-glutamine gamma-glutamyltransferase e protein	0.033	2.547
D3zsh7	Col17a1	Collagen alpha-1(xvii) chain	0.002	2.485
D3zjk2	Serpinb3a	Protein serpinb3a	0.038	2.445
Q6ie17	Stfa2l2	Stefin-3	0.005	2.439
Q5u206	Calml3	Calmodulin-like protein 3	0.013	2.429
Q4v885	Colec12	Collectin-12	0.017	0.547
D3zqi1	Gpx7	Glutathione peroxidase 7 precursor	0.036	0.541

Table IV. Continued.

Protein ID	Gene name	Protein name	P-value	Fold change
D3z9m5	Fkbp7	Peptidyl-prolyl cis-trans isomerase fkbp7 precursor	0.014	0.530
O88201	Clec11a	C-type lectin domain family 11 member a	0.047	0.529
D3zrd3	Pde6d	Retinal rod rhodopsin-sensitive cgmp 3',5'-cyclic phosphodiesterase subunit delta	0.009	0.528
P21807	Prph	Peripherin	0.008	0.527
G3v6m4	Capn6	Calpain-6	0.024	0.514
D3zg88	Sssca1	Sjogren syndrome/scleroderma autoantigen 1 homolog	0.034	0.502
Q2eja0	Yap1	Yorkie homolog	0.002	0.494
Q3b7u1	Maged2	Melanoma-associated antigen d2	0.003	0.492
O35276	Nrp2	Neuropilin-2	0.015	0.491
D3zun5	Pofut2	Gdp-fucose protein o-fucosyltransferase 2 precursor	0.018	0.490
P70583; d4a6v3	Dut	Deoxyuridine 5'-triphosphate nucleotidohydrolase	0.021	0.489
P19527	Nefl	Neurofilament light polypeptide	0.026	0.479
M0r649	Exoc4	Exocyst complex component 4	0.031	0.466
Q99pd6	Tgfb1i1	Transforming growth factor beta-1-induced transcript 1 protein	0.048	0.466
P54001	P4ha1	Prolyl 4-hydroxylase subunit alpha-1	0.019	0.461
D3zt07	Sept5	Septin-5	0.046	0.452
P12839; g3v7s2	Nefm	Neurofilament medium polypeptide	0.020	0.444
B5df50	Galnt2	Polypeptide n-acetylgalactosaminyltransferase 2	0.038	0.436
D3zuq0	Rilpl1	Rilp-like protein 1	0.041	0.418
D4a8h3	Uba6	Ubiquitin-like modifier-activating enzyme 6	0.024	0.415
D4a9u4	Eln	Elastin	0.041	0.409
D4ad75	Dpy19l1	Protein dpy-19 homolog 1	0.014	0.408
Q6p7d4	Cyp20a1	Cytochrome p450 20a1	0.007	0.406
Q5xi28	Raver1	Ribonucleoprotein ptb-binding 1	0.045	0.398
P09117	Aldoc	Fructose-bisphosphate aldolase c	0.004	0.396
D3zct5	Pald1	Paladin	0.004	0.395
A1l1k3	Anapc5	Anaphase-promoting complex subunit 5	0.028	0.392
P62966	Crabp1	Cellular retinoic acid-binding protein 1	0.016	0.384
Q569b7	Rwdd4	Rwd domain-containing protein 4	0.040	0.384
Q5hze4	Mri1	Methylthioribose-1-phosphate isomerase	0.011	0.376
F1lqz3	Kif3a	Kinesin family member 3a	0.011	0.376
O88752	Hbe1	Hemoglobin, epsilon 1	0.033	0.375
Q5u1z0	Rab3gap2	Rab3 gtpase-activating protein non-catalytic subunit	0.003	0.373
A1a5r1	Rbfox1	Fox-1 homolog c	0.033	0.366
D4a845	Rpa3	Replication protein a 14 kda subunit	0.021	0.366
D3zwc6	Sntb1	Beta-1-syntrophin	0.003	0.365
G3v8m1	Pold1	Dna polymerase delta catalytic subunit	0.003	0.353
P23565	Ina	Alpha-internexin	0.039	0.352
Q4klk9	Ssu72	Rna polymerase ii subunit a c-terminal domain phosphatase ssu72	0.025	0.349
F1mah6	Cdh11	Cadherin 11	0.007	0.326
Q6ayg3	Prune	Prune homolog (drosophila) (ec:3.6.1.1)	0.001	0.278
P04638	Apoa2	Apolipoprotein a-ii	0.010	0.270
Q9z2z8	Dhcr7	7-dehydrocholesterol reductase	0.000	0.221
Q10758	Krt8	Keratin, type ii cytoskeletal 8	0.002	0.214
Q812d3	Ppil3	Peptidyl-prolyl cis-trans isomerase-like 3	0.000	0.188
G3v8r3	Hbz	Hemoglobin, zeta	0.004	0.128
B5dfl9	Sestd1	Sec14 and spectrin domains 1	0.000	0.065
Q9eph1	A1bg	Alpha-1b-glycoprotein	0.016	0.033

Group 1, upper-left lip of fetus at 72 h after modeling in GA16.5 rats; Group 3, upper-left lip of fetus at 72 h after modeling in GA18.5 rats. GA, gestational age.

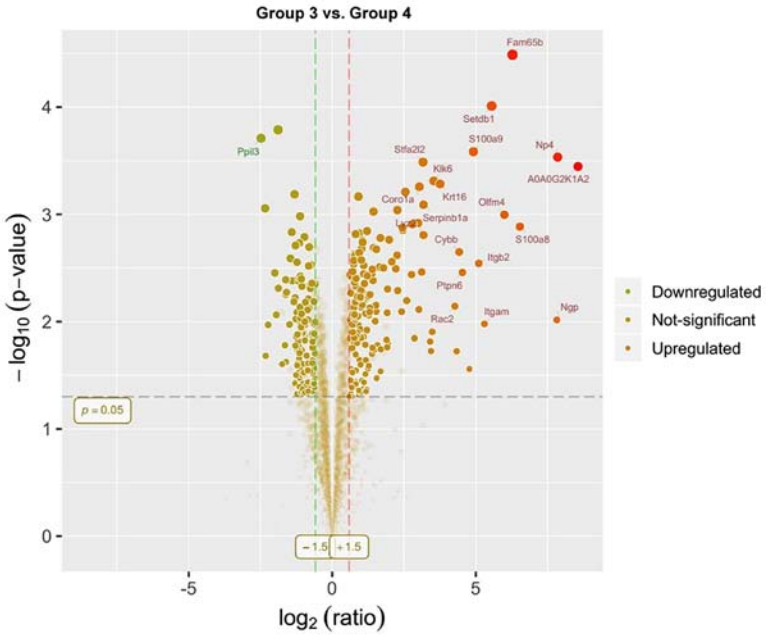

Figure 11. Volcano plot of the differentially expressed proteins in group 3 and group 4. Group 3, upper-left lip of fetus at 72 h after modeling in GA18.5 rats; Group 4, upper-right lip of fetus at 72 h after modeling in GA18.5 rats. GA, gestational age.

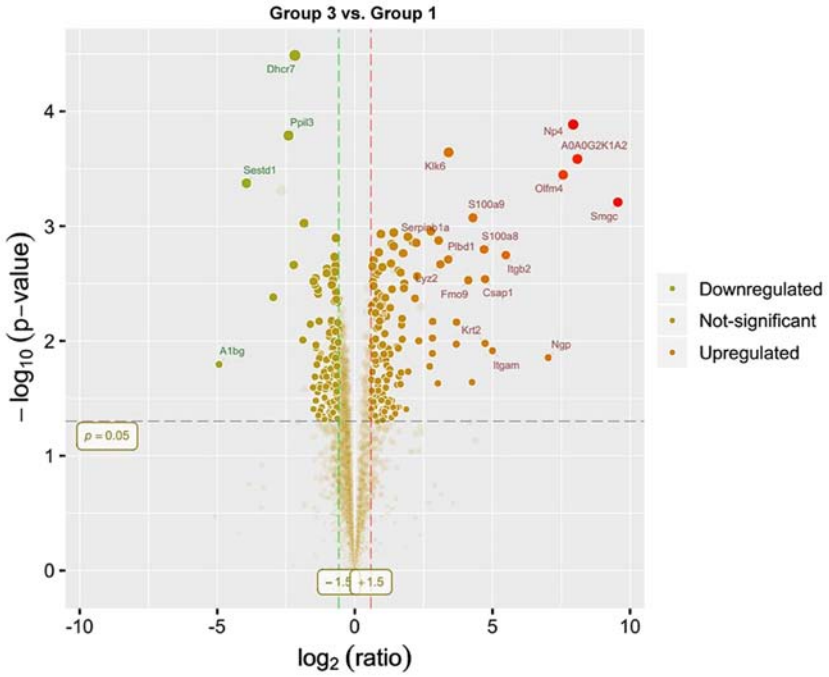

Figure 12. Volcano plot of the differentially expressed proteins in group 3 and group 1. Group 1, upper-left lip of fetus at 72 h after modeling in GA16.5 rats; Group 3, upper-left lip of fetus at 72 h after modeling in GA18.5 rats. GA, gestational age.

RT-qPCR analysis of possible target protein in cleft lip repair. RNA was extracted from tissue samples with TRIzol® reagent and the quality was checked using gel electrophoresis. Relative mRNA levels were analyzed using RT-qPCR (Fig. 16). The relative mRNA expression levels of Smad4 were significantly higher in group 2, compared with group 1 (P<0.05). Moreover, the relative mRNA expression levels of Fabp5 were significantly lower in groups 4 and 1, compared with group 3 (P<0.05). Additionally, the relative mRNA expression levels of S100a4 were significantly lower in group 4, compared with group 3 (P<0.05). S100a8 and S100a9 were significantly higher in group 3, compared with in groups 1 and 4 (P<0.05).

Immunofluorescence results. Immunofluorescence staining of Smad4, Fabp5, S100a4, S100a8 and S100a9 was performed on samples from both the GA16.5 and GA18.5 groups 72 h post-surgery. The expression levels of all five proteins increased in GA18.5 compared to GA16.5, and the differences were statistically significant (P<0.05; Fig. 17).

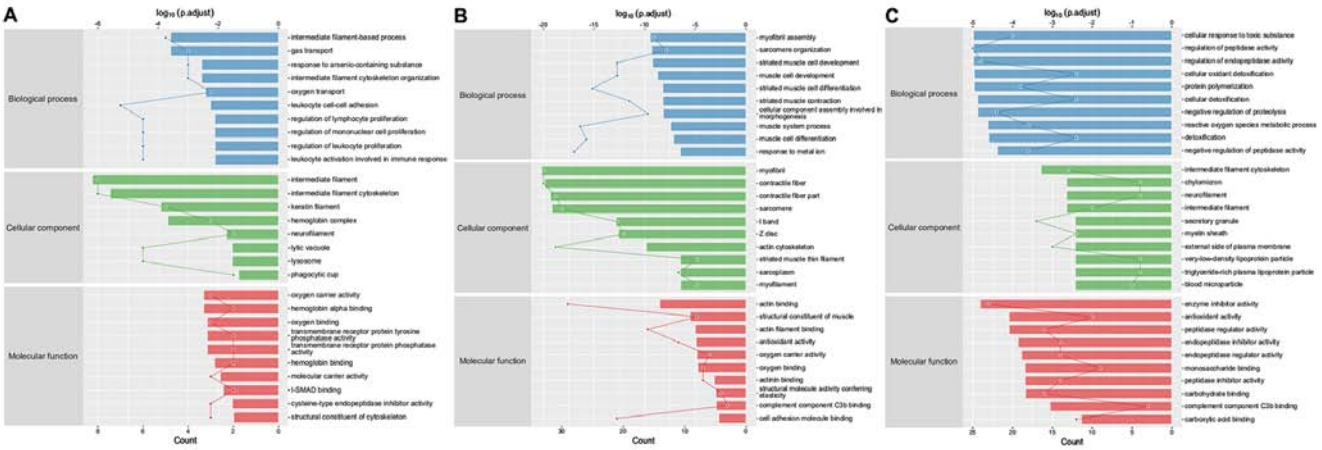

Figure 13. GO enrichment analysis of the differentially expressed proteins. GO enrichment analysis of the differentially expressed proteins in (A) group 1 and group 2, (B) in group 3 and group 4 and (C) in group 3 and group 1. GA, gestational age; GO, Gene Ontology; p.adjust, adjusted P-value. Group 1, upper-left lip of fetus at 72 h after modeling in GA16.5 rats; Group 2, upper-right lip of fetus at 72 h after modeling in GA16.5 rats; Group 3, upper-left lip of fetus at 72 h after modeling in GA18.5 rats; Group 4, upper-right lip of fetus at 72 h after modeling in GA18.5 rats. GA, gestational age.

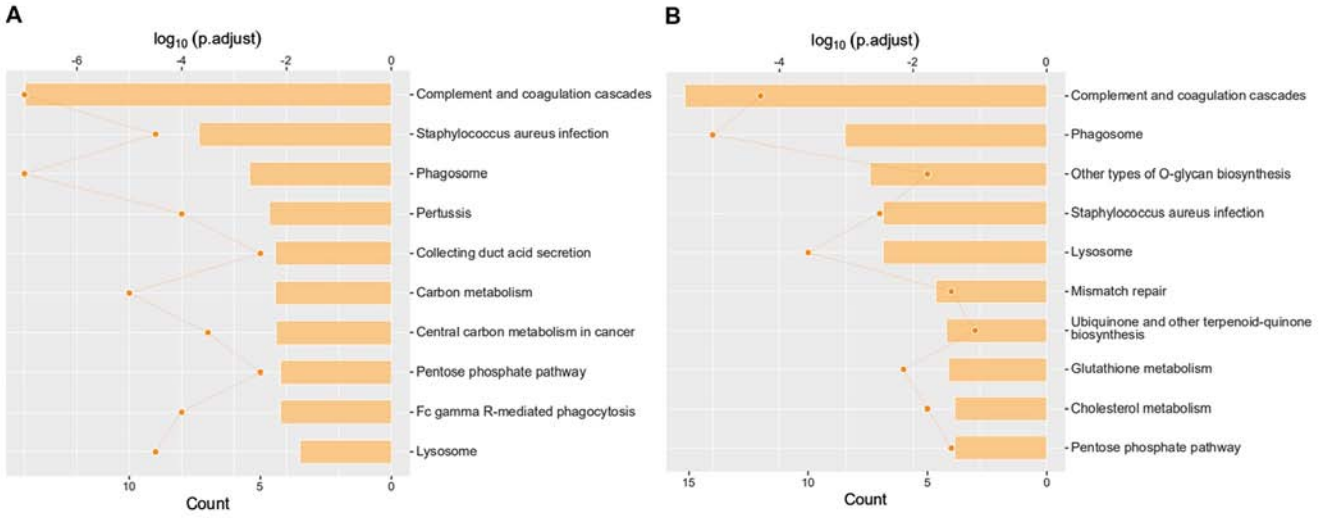

Figure 14. KEGG pathway enrichment analysis of the differentially expressed proteins. KEGG pathway enrichment analysis of the differentially expressed proteins in (A) group 3 and group 4 and (B) in group 3 and group 1. GA, gestational age; KEGG, Kyoto Encyclopedia of Genes and Genomes; p.adjust, adjusted P-value. Group 1, upper-left lip of fetus at 72 h after modeling in GA16.5 rats; Group 2, upper-right lip of fetus at 72 h after modeling in GA16.5 rats; Group 3, upper-left lip of fetus at 72 h after modeling in GA18.5 rats; Group 4, upper-right lip of fetus at 72 h after modeling in GA18.5 rats. GA, gestational age.

PRM analysis of differential protein expression. The differences in multiple variations of Smad4 expression were compared between groups 1 and 2. The panel reaction monitoring calculated this difference as 0.557, indicating downregulation in group 1 compared with in group 2 (P=0.043) (Table II). In contrast, no statistically significant differences were observed between groups 3 and 4. The difference in multiple variations of Fabp5 between groups 3 and 4 was calculated as 2.91, indicating upregulation in group 3 compared with in group 4 (P=0.024) (Table III). Additionally, the expression levels of Fabp5 were upregulated (P=0.01) in group 3 compared with in group 1; however, the difference between the variations present in groups 1 and 2 was not statistically significant. The difference in the multiple variations of S100a4 and S100a8 between groups 3 and 4 was calculated as 2.897 and 92.828, respectively, indicating an upregulation of the expression levels of both proteins in group 3 (P=0.001 and P=0.002, respectively) (Table III). Furthermore, the difference in the multiple variations of S100a8 between groups 3 and 1 was 25.933, which indicates upregulation in group 3 (P=0.002) (Table IV). However, the differences were not statistically significant between groups 1 and 2. The difference in the multiple variations of S100a9 was 30.191 and 19.538 between groups 3 and 4 and groups 3 and 1, respectively, suggesting upregulation in group 3 (P=0.0004 and P=0.001, respectively) (Tables III and IV). In contrast, the difference in the multiple variations of S100a9 between groups 1 and 2 was not statistically significant (Tables II-IV).

Discussion

In recent decades, various animal models of congenital cleft lip have been successfully established through surgical induction (4,20). It has been suggested that intrauterine cleft

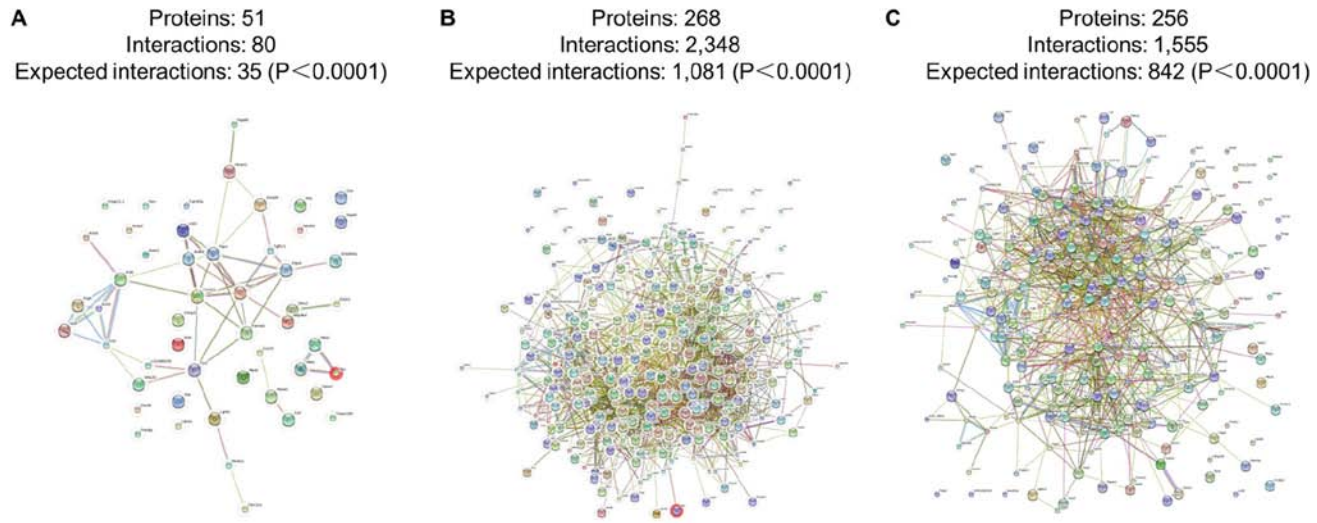

Figure 15. Interaction network of differentially expressed proteins. Interaction network of differentially expressed proteins in (A) group 1 and group 2, (B) 3 and group 4 and (C) 3 and group 1. Group 1, upper-left lip of fetus at 72 h after modeling in GA16.5 rats; Group 2, upper-right lip of fetus at 72 h after modeling in GA16.5 rats; Group 3, upper-left lip of fetus at 72 h after modeling in GA18.5 rats; Group 4, upper-right lip of fetus at 72 h after modeling in GA18.5 rats. GA, gestational age.

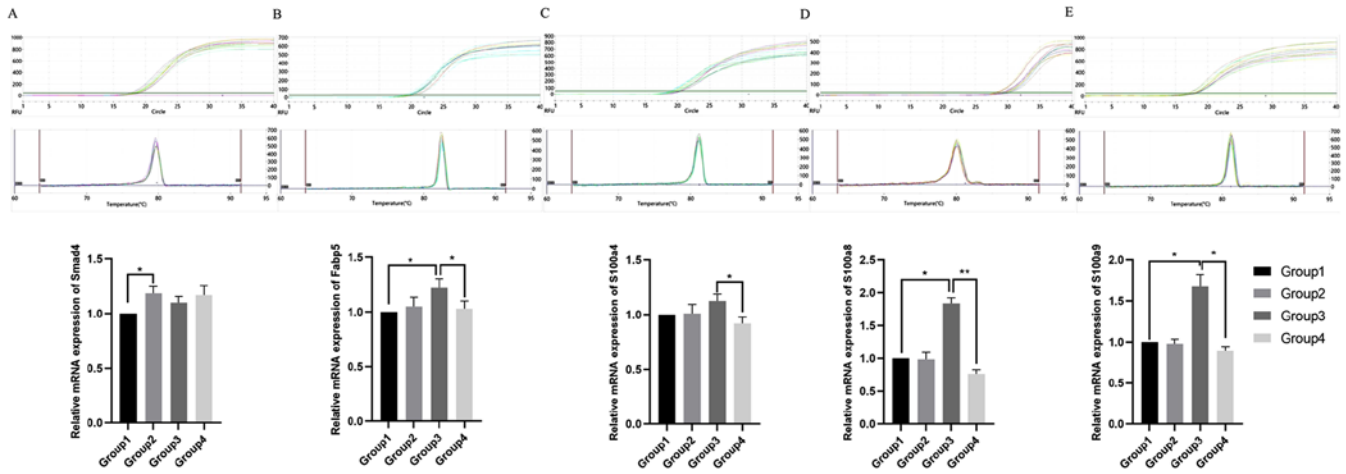

Figure 16. RT-qPCR analysis of Smad4, Fabp5, S100a4, S100a8 and S100a9. RT-qPCR detection and amplification of (A) Smad4, (B) Fabp5, (C) S100a4, (D) S100a8 and (E) S100a9. The dissolution curves and relative mRNA expression levels are shown for each target. RT-qPCR, reverse transcription-quantitative PCR; Fabp5, fatty acid binding protein 5; Smad4, Smad family member 4; S100, S100 calcium binding protein. Group 1, upper-left lip of fetus at 72 h after modeling in GA16.5 rats; Group 2, upper-right lip of fetus at 72 h after modeling in GA16.5 rats; Group 3, upper-left lip of fetus at 72 h after modeling in GA18.5 rats; Group 4, upper-right lip of fetus at 72 h after modeling in GA18.5 rats. *P<0.05; **P<0.01. GA, gestational age.

lip repair can effectively improve this defect and reduce the impact of scars on normal facial development after birth. Thus, it also provides a new way for the effective repair of congenital cleft lips. In the present study, pregnant SD rats were used to establish a fetal rat model of cleft lip wound at two time points, GA16.5 and GA18.5. The different pregnancy models were induced by using two different repair methods of a cleft lip wound of the fetus (21,22). The exact gestational age is particularly important for the results of the repair of cleft lip in the fetal rats. Thus, the use of a rat model provides an added advantage in that the exact time of conception can be replicated, thereby minimizing differences between groups.

The present findings confirmed the hypothesis that fetal rat defects can be regenerated during early pregnancy without scar formation (23). It was also demonstrated that fetal rat defects could not be completely regenerated in late pregnancy and resulted in scarring (24). Furthermore, the expression of pro-inflammatory factors was different between the two groups. However, these observations were only made at one time point (72 h) after constructing cleft lip wounds in fetal rats. Future studies are needed to examine samples collected at different time points following surgery. Another shortcoming of this study entails the lack of comparison between the cleft lip wound repairs of fetal rats at different ages, such as the fetus in the early stages of pregnancy, or in newborn and/or adult rats. Label-free quantitative proteomics were used to examine proteins that play important roles in the postoperative repair process of fetal cleft lip. Protein expression was examined in four groups of samples. In addition, bioinformatics analysis was conducted to identify potential

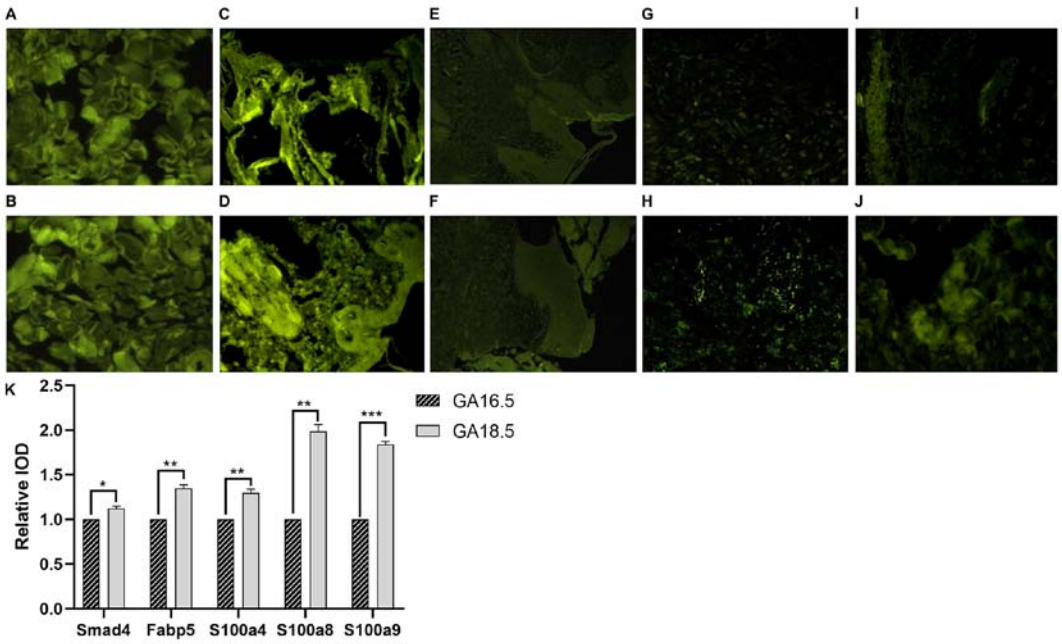

Figure 17. Immunofluorescence analysis Smad4, Fabp5, S100a4, S100a8 and S100a9. (A and B) Smad4 staining of upper lip tissue from (A) the GA16.5 group and (B) the GA18.5 group. (C and D) Fabp5 staining of upper lip tissue from (C) the GA16.5 group and (D) the GA18.5 group. (E and F) S100a4 staining of upper lip tissue from (F) the GA16.5 group and (F) the GA18.5 group. (G and H) S100a8 staining of upper lip tissue from (G) the GA16.5 group and (H) the GA18.5 group. (I and J) S100a9 staining of upper lip tissue from (I) the GA16.5 group and (J) the GA18.5 group. (K) Relative IOD values for Smad4, Fabp5, S100a4, S100a8 and S100a9 staining. *P<0.05; **P<0.01; ***P>0.001. Fabp5, fatty acid binding protein 5; Smad4, Smad family member 4; S100, S100 calcium binding protein; IOD, integral optical density; GA, gestational age.

biological markers, providing a theoretical reference and methodological basis for the examination of relevant mechanisms underlying fetal intrauterine scar repair. However, further studies are required to determine whether any one protein or several proteins, plays a key role in wound healing.

Smad4 belongs to the family of Smad proteins and is a common mediator in the signal transduction processes of the TGF-β family (25). TGF-β expression can lead to fibroblast proliferation and ECM deposition (26,27). The present findings indicated that the mRNA and protein expression levels of Smad4 were downregulated in the scar-free repair group.

Furthermore, the mRNA and protein expression levels of Fabp5 were upregulated in the scar formation group. Therefore, it may be hypothesized that Fabp5 could be involved in the fibrosis of the fetal cleft lip wound, which may be mediated by the TGF-β signaling pathway (28-30).

S100a4 is a member of the S100 calcium-binding protein family, and its expression is associated with various non-neoplastic diseases, such as chronic obstructive pulmonary disease and cardiac hypertrophy (31-35). The present study demonstrated that the mRNA and protein expression levels of S100a4 were upregulated in the scar formation group, which may be associated with scar repair of fetal rat cleft lip wounds.

S100a8 is also a member of the S100 calcium-binding protein family (36-42). mRNA and protein expression levels of S100a8 were significantly upregulated in the scar repair group in the present study, indicating a potential role for S100a8 in the process of fetal cleft lip wound healing.

Current reports frequently associate S100a9, a member of the calcium-binding protein family S100, with infectious diseases, immune diseases and tumors, such as non-small cell lung adenocarcinoma (43-45). mRNA and protein expression levels of S100a9 were significantly upregulated in the scar formation group. Therefore, we speculated that S100a9 may play an important role in the process of fetal wound healing. However, whether the reduced expression levels of Fabp5, S100a4, S100a8 and S100a9 in the third trimester of pregnancy would reduce or worsen scar formation remains unclear. Further functional testing and regulatory studies are required to confirm the role of these five differentially expressed proteins in fetal wound repair.

The cleft lip is a very common congenital condition that often leaves life-long scarring. The present study identified five differentially expressed proteins, namely Smad4, Fabp5, S100a4, S100a8 and S100a9, that may be potential biomarkers of the scarless repair process in fetal rat cleft lip wounds. These findings may facilitate the discovery of new clinical targets for the prevention and treatment of scars. However, the role of these proteins in fetal wound repair and potential underlying mechanisms require further examination.

Acknowledgements

Not applicable.

Funding

The present study was supported by a grant from the National Science and Basic Resources Survey Special Foundation, China (grant no. 2017FY101204), the Technology Innovation Guide Program of Hunan Province, China (grant no. 2017SK50124), the Science and Technology Major Project of Hunan Province, China (grant no. 2019SK1010) and

the Science and Technology Major Project of Hunan Province, China (grant no. 2019SK1015).

Availability of data and materials

The datasets used and/or analyzed during the current study are available from the corresponding author on reasonable request.

Authors' contributions

YY, FH and JZho conceived and designed research. YY and FH performed animal experiments and staining. YY, HL, PJ, FH, JY, KG, SH and JZha performed PCR and label-free quantification PRM. YY, FH, JC, JY, ZC, AW and JZha analyzed data. YY and FH prepared figures. YY drafted the manuscript. FH and JZho edited and revised the manuscript. YY, FH, HL AW, PJ and JZho approved the final version of the manuscript. FH and JZho confirmed the authenticity of all of the raw data. All authors read and approved the final manuscript.

Ethics approval and consent to participate

This study followed the regulations stipulated by the People's Republic of China regarding the Management of Experimental Animals and was approved by The Animal Experiment Management and Medical Ethics Sub-committee of The Third Xiangya Hospital of Central South University, Hunan, China (approval no. 2014-S168).

Patient consent for publication

Not applicable.

Competing interests

The authors declare that they have no competing interests.

References

1. VanKoevering KK, Morrison RJ, Prabhu SP, Torres MF, Mychaliska GB, Treadwell MC, Hollister SJ and Green GE: Antenatal three-dimensional printing of aberrant facial anatomy. Pediatrics 136: e1382-e1385, 2015.
2. Burrington JD: Wound healing in the fetal lamb. J Pediatr Surg 6: 523-528, 1971.
3. Beanes SR, Hu FY, Soo C, Dang CM, Urata M, Ting K, Atkinson JB, Benhaim P, Hedrick MH and Lorenz HP: Confocal microscopic analysis of scarless repair in the fetal rat: Defining the transition. Plast Reconstr Surg 109: 160-170, 2002.
4. Walmsley GG, Hu MS, Hong WX, Maan ZN, Lorenz HP and Longaker MT: A mouse fetal skin model of scarless wound repair. J Vis Exp 16: 52297, 2015.
5. Dang CM, Beanes SR, Lee H, Zhang X, Soo C and Ting K: Scarless fetal wounds are associated with an increased matrix metalloproteinase-to-tissue-derived inhibitor of metalloproteinase ratio. Plast Reconstr Surg 111: 2273-2285, 2003.
6. Longaker MT, Whitby DJ, Adzick NS, Crombleholme TM, Langer JC, Duncan BW, Bradley SM, Stern R, Ferguson MW and Harrison MR: Studies in fetal wound healing, VI. Second and early third trimester fetal wounds demonstrate rapid collagen deposition without scar formation. J Pediatr Surg 25: 63-69, 1990.
7. Lorenz HP, Whitby DJ, Longaker MT and Adzick NS: Fetal wound healing. The ontogeny of scar formation in the non-human primate. Ann Surg 217: 391-396, 1993.
8. Cass D, Bullard KM, Sylvester KG, Yang EY, Longaker MT and Adzick NS: Wound size and gestational age modulate scar formation in fetal wound repair. J Pediatr Surg 32: 411-415, 1997.
9. Longaker MT and Adzick NS: The biology of fetal wound healing: A review. Plast Reconstr Surg 87: 788-798, 1991.
10. Armstrong JR and Ferguson MW: Ontogeny of the skin and the transition from scar-free to scarring phenotype during wound healing in the pouch young of a marsupial, Monodelphis domestica. Dev Biol 169: 242-260, 1995.
11. Stern M, Dodson TB, Longaker MT, Lorenz HP, Harrison MR and Kaban LB: Fetal cleft lip repair in lambs: Histologic characteristics of the healing wound. Int J Oral Maxillofac Surg 22: 371-374, 1993.
12. Longaker MT, Dodson TB and Kaban LB: A rabbit model for fetal cleft lip repair. J Oral Maxillofac Surg 48: 714-719, 1990.
13. Oberg KC, Evans ML, Nguyen T, Peckham NH, Kirsch WM and Hardesty RA: Intrauterine repair of surgically created defects in mice (lip incision model) with a microclip: Preamble to endoscopic intrauterine surgery. Cleft Palate Craniofac J 32: 129-137, 1995.
14. Hu F, Yan Y, Wang CW, Liu Y, Wang JJ, Zhou F, Zeng QH, Zhou X, Chen J, Wang AJ and Zhou JD: Article effect and mechanism of ganoderma lucidum polysaccharides on human fibroblasts and skin wound healing in mice. Chin J Integr Med 25: 203-209, 2019.
15. Xue YN, Yan Y, Chen ZZ, Chen J, Tang FJ, Xie HQ, Tang SJ, Cao K, Zhou X, Wang AJ and Zhou JD: LncRNA TUG1 regulates FGF1 to enhance endothelial differentiation of adipose-derived stem cells by sponging miR-143. J Cell Biochem 120: 19087-19097, 2019.
16. Guo H, Chen T, Liang Z, Fan L, Shen Y and Zhou D: iTRAQ and PRM-based comparative proteomic profiling in gills of white shrimp Litopenaeus vannamei under copper stress. Chemosphere 263: 128270, 2021.
17. Chen PS, Li YP and Ni HF: Morphology and evaluation of renal fibrosis. Adv Exp Med Biol 1165: 17-36, 2019.
18. Luo Y, Yan Y, Zhang S and Li Z: Computational approach to investigating key GO terms and KEGG pathways associated with CNV. Biomed Res Int 2018: 8406857, 2018.
19. Dong X, Landford WN, Hart J, Risolino M, Kaymakcalan O, Jin J, Toyoda Y, Ferretti E, Selleri L and Spector JA: Toward microsurgical correction of cleft lip ex utero through restoration of craniofacial developmental programs. Plast Reconstr Surg 140: 75-85, 2017.
20. Stelnicki EJ, Lee S, Hoffman W, Lopoo J, Foster R, Harrison MR and Longaker MT: A long-term, controlled-outcome analysis of in utero versus neonatal cleft lip repair using an ovine model. Plast Reconstr Surg 104: 607-615, 1999.
21. Harling TR, Stelnicki EJ, Hedrick MH and Longaker MT: In utero models of craniofacial surgery. World J Surg 27: 108-116, 2003.
22. Mast BA, Haynes JH, Krummel TM, Diegelmann RF and Cohen IK: In vivo degradation of fetal wound hyaluronic acid results in increased fibroplasia, collagen deposition, and neovascularization. Plast Reconstr Surg 89: 503-509, 1992.
23. Frantz FW, Diegelmann RF, Mast BA and Cohen IK: Biology of fetal wound healing: Collagen biosynthesis during dermal repair. J Pediatr Surg 27: 945-949, 1992.
24. Wilgus TA: Regenerative healing in fetal skin: A review of the literature. Ostomy Wound Manage 53: 16-33, 2007.
25. Hu HH, Chen DQ, Wang YN, Feng YL, Cao G, Vaziri ND and Zhao YY: New insights into TGF-beta/Smad signaling in tissue fibrosis. Chem Biol Interac 292: 76-83, 2018.
26. Honardoust D, Ding J, Varkey M, Shankowsky HA and Tredget EE: Deep dermal fibroblasts refractory to migration and decorin-induced apoptosis contribute to hypertrophic scarring. J Burn Care Res 33: 668-677, 2012.
27. Wu C, Jiang J, Boye A, Jiang Y and Yang Y: Compound Astragalus and Salvia miltiorrhiza extract suppresses rabbits' hypertrophic scar by modulating the TGF-β/Smad signal. Dermatology 229: 363-368, 2014.
28. Furuhashi M, Ogura M, Matsumoto M, Yuda S, Muranaka A, Kawamukai M, Omori A, Tanaka M, Moniwa N, Ohnishi H, *et al*: Serum FABP5 concentration is a potential biomarker for residual risk of atherosclerosis in relation to cholesterol efflux from macrophages. Sci Rep 7: 217, 2017.
29. Yeung DC, Wang Y, Xu A, Cheung SC, Wat NM, Fong DY, Fong CH, Chau MT, Sham PC and Lam KS: Epidermal fatty-acid-binding protein: A new circulating biomarker associated with cardio-metabolic risk factors and carotid atherosclerosis. Eur Heart J 29: 2156-2163, 2008.

30. Song J, Zhang H, Wang Z, Xu W, Zhong L, Cao J, Yang J, Tian Y, Yu D, Ji J, *et al*: The role of FABP5 in radiation-induced human skin fibrosis. Radiat Res 189: 177-186, 2018.
31. Fei F, Qu J, Li C, Wang X, Li Y and Zhang S: Role of metastasis-induced protein S100A4 in human non-tumor pathophysiologies. Cell Biosci 7: 64, 2017.
32. Grotterød I, Maelandsmo GM and Boye K: Signal transduction mechanisms involved in S100A4-induced activation of the transcription factor NF-kappaB. BMC Cancer 10: 241, 2010.
33. Schneider M, Kostin S, Strøm CC, Aplin M, Lyngbaek S, Theilade J, Grigorian M, Andersen CB, Lukanidin E, Lerche Hansen J and Sheikh SP: S100A4 is upregulated in injured myocardium and promotes growth and survival of cardiac myocytes. Cardiovasc Res 75: 40-50, 2007.
34. Tomcik M, Palumbo-Zerr K, Zerr P, Avouac J, Dees C, Sumova B, Distler A, Beyer C, Cerezo LA, Becvar R, *et al*: S100A4 amplifies TGF-β-induced fibroblast activation in systemic sclerosis. Ann Rheum Dis 74: 1748-1755, 2015.
35. Zhao YX, Ho CK, Xie Y, Chen YH, Li HZ, Zhang GY and Li QF: Calcimycin suppresses S100A4 expression and inhibits the stimulatory effect of transforming growth factor β1 on Keloid fibroblasts. Ann Plast Surg 81: 163-169, 2018.
36. Donato R: Intracellular and extracellular roles of S100 proteins. Microsc Res Tech 60: 540-551, 2003.
37. Lin H, Andersen GR and Yatime L: Crystal structure of human S100A8 in complex with zinc and calcium. BMC Struct Biol 16: 8, 2016.
38. Bouzidi F and Doussiere J: Binding of arachidonic acid to myeloid-related proteins (S100A8/A9) enhances phagocytic NADPH oxidase activation. Biochem Biophys Res Commun 325: 1060-1065, 2004.
39. Gebhardt C, Németh J, Angel P and Hess J: S100A8 and S100A9 in inflammation and cancer. Biochem Pharmacol 72: 1622-1631, 2006.
40. Basso D, Bozzato D, Padoan A, Moz S, Zambon CF, Fogar P, Greco E, Scorzeto M, Simonato F, Navaglia F, *et al*: Inflammation and pancreatic cancer: Molecular and functional interactions between S100A8, S100A9, NT-S100A8 and TGFβ1. Cell Commun Signal 26: 12-20, 2014.
41. Shabani F, Farasat A, Mahdavi M and Gheibi N: Calprotectin (S100A8/S100A9): A key protein between inflammation and cancer. Inflamm Res 67: 801-812, 2018.
42. Yaundong L, Dongyan W, Lijun H and Zhibo X: Effects of downregulation of S100A8 protein expression on cell cycle and apoptosis of fibroblasts derived from hypertrophic scars. Aesthet Surg J 34: 160-167, 2014.
43. Hessian PA, Edgeworth J and Hogg N: MRP-8 and MRP-14, two abundant Ca (2+)-binding proteins of neutrophils and monocytes. J Leukoc Biol 53: 197-204, 1993.
44. Markowitz J and Carson WE III: Review of S100A9 biology and its role in cancer. Biochim Biophys Acta 1835: 100-109, 2013.
45. Zhong A, Xu W, Zhao J, Xie P, Jia S, Sun J, Galiano RD, Mustoe TA and Hong SJ: S100A8 and S100A9 are induced by decreased hydration in the epidermis and promote fibroblast activation and fibrosis in the dermis. Am J Pathol 186: 109-122, 2016.